scientific reports

Check for updates

OPEN

Effect of environmental factors on adsorption of ciprofloxacin from wastewater by microwave alkali modified fly ash

Tonglinxi Liu[1], Wen Liu[2], Xinyue Li[1,3], Hanyu Wang[1], Yushan Lan[1], Shengmin Zhang[1]✉, Yujun Wang[1]✉ & Huiqing Liu[1]

Antibiotics, as emerging persistent pollutants, pose significant threats to human health. The effective and low-cost removal of ciprofloxacin (CIP) from wastewater has become an important research focus. In this study, fly ash (FA) was used as the raw material, and modified fly ash (MFA) was prepared by varying microwave power, alkali concentration, and immersion time to investigate its adsorption characteristics for CIP. Results showed that the optimal preparation conditions for MFA with the most effective adsorption of CIP, using the Box-Behnken response surface methodology, were a microwave power of 480 W, an alkali concentration of 1.5 mol/L, and a modification time of 3 h. Scanning electron microscopy, Fourier transform infrared spectroscopy, and X-ray diffraction analyses revealed that after modification, the glassy structure of FA is destroyed, the specific surface area is increased, and obvious hydroxyl O–H absorption peaks appear. Both FA and MFA exhibited adsorption processes for CIP that conformed to pseudo-second-order kinetics and the Langmuir equation. Maximum adsorption of CIP (9.61 and 12.67 mg/g) was achieved at pH = 6. With increasing temperature, the adsorption capacity of both FA and MFA for CIP decreased, indicating an exothermic process. The adsorption capacity of CIP decreased with increasing ion concentration, with the impact order of ions being $Al^{3+} > Ca^{2+} > Na^{+}$. The results show that pore filling, electrostatic interaction, ion exchange and complexation are the main ways of CIP adsorption by FA. Microwave alkali modified fly ash is an economical and efficient adsorbent for CIP removal in water, realizing the purpose of "treating waste with waste". This study provides a scientific basis for controlling CIP treatment in wastewater.

Keywords Fly ash, Microwave-alkali modification, Response surface optimization, Ciprofloxacin, Adsorption mechanism

Antibiotics, as commonly used pharmaceuticals, have been extensively applied in medical treatment, livestock breeding, and aquaculture[1,2]. However, their limited bio-availability has led to inevitable accumulation of antibiotic residues in surface water[3], groundwater[4], soil[5], and sediment[6], posing potential risks to ecosystems and human health. Among various antibiotics, ciprofloxacin (CIP) is one of the most commonly detected antibiotics in environmental matrices due to its high usage and low removal efficiency[7,8]. It was found that the highest concentration of CIP in pharmaceutical wastewater, municipal wastewater, surface water, and groundwater reached 31 mg/L, 14 mg/L, 2.5 mg/L, and 0.014 mg/L, respectively[9]. Prolonged exposure to elevated levels of CIP can cause health problem in humans and animals, including reproductive problems, liver damage, and central nervous system abnormalities in both humans and animals[10]. The removal of CIP from wastewater to prevent its prolonged environmental presence and subsequent impacts on terrestrial and aquatic ecosystems has become an important research focus[11].

Currently, various methods are employed to address CIP contamination in wastewater[12], including adsorption[13], photocatalysis[14] membrane filtration[15], and electrochemical techniques[16]. Among these, adsorption is considered one of the more economical treatment technologies due to its advantages such as wide availability of raw materials[17], simplicity of operation, low cost, high efficiency, and minimal secondary pollution[18,19]. The selection of adsorption materials is particularly crucial due to the varying physic-chemical properties of

[1]College of Resources and Environment, Jilin Agricultural University, Changchun 130118, China. [2]Zhaoming (Shandong) Ecological and Environmental Development Co., Ltd, Jinan 250014, China. [3]College of Environment, Beijing Jiaotong University, Beijing 100044, China. ✉email: zhangshengmin@jlau.edu.cn; yujunw@jlau.edu.cn

different wastewaters. Prominent frontiers in adsorption materials include mineral materials (zeolites, fly ash, etc.), carbon-based materials (activated carbon, biochar, etc.), metal oxide materials (magnetic iron oxides, iron–manganese oxides, etc.), biopolymer materials (chitosan, natural rubber, etc.), and nanomaterials (carbon nanotubes, etc.)[20]. Among them, fly ash (FA) possesses a porous structure and contains substances such as SiO_2 and Al_2O_3 on its surface, making it exhibit excellent adsorption properties for heavy metals and organic compounds[21]. Therefore, it can serve as a favorable adsorbent material due to its low cost and its ability to reduce environmental pollution, thereby achieving the goal of "treating waste with waste".

FA is a significant industrial waste in China and has a low economic reuse rate. If not effectively utilized, it can damage large areas of land and contribute to environmental pollution[22]. Currently, there is increasing global attention to convert FA into an efficient adsorbent for removing pollutants from the environment[23]. The use of primitive FA as an adsorbent for pollutants is not effective[24]. To improve its efficiency, various physical and chemical methods have been introduced to activate and modify the chemical composition and physical properties of FA. The commonly used modifications include acid or alkali modification, microwave-alkali modification, and others. Modified FA exhibits efficient adsorption capacity for pollutants found in wastewater, including metal ions, dyes, volatile organic compounds and on antibiotics[25], among others[26]. Microwave modification can improve the adsorption capacity of the material. Microwave can cause the carbon structure to expand inward, which enhances the escape of volatile substances and strengthens the pore structure of the material[27]. After alkali modification, the active sites of FA are stimulated by (SiO_2 and Al_2O_3), resulting in increased surface roughness and surface area[28]. As a result, the adsorption of norfloxacin is enhanced[29]. However, there is still a lack of research on the optimal parameters for preparing modified fly ash (MFA) with the best adsorption performance for antibiotics, especially CIP under the complex toxic effects in aquatic environments. Additionally, studies on the adsorption mechanism of antibiotics by MFA and its influencing factors remain insufficient.

Given the above-mentioned issues, the objectives of this study are to: (1) investigate the optimal conditions for preparing microwave-alkali modified fly ash with the best adsorption performance and characterize the differences; (2) explore the effects of different factors on the adsorption characteristics of ciprofloxacin by modified fly ash; (3) elucidate the adsorption capacity and mechanism of antibiotics by modified fly ash. By analyzing the adsorption mechanism of MFA on CIP and the effects of different environmental factors on CIP adsorption, it provides a scientific basis for controlling CIP in wastewater.

Materials and methods

Reagents

The reagents used in the experiments, including NaOH, HCl, $Ca(OH)_2$, etc., were all of analytical grade. Deionized water was used throughout the experiments. CIP ($C_{17}H_{18}FN_3O_3$), purchased from Aladdin Reagent Company, has a density of 1.461 g/cm^3 and appears as white or off-white crystalline powder. A certain amount of CIP was dried at 105 °C for 2 h, accurately weighed (1.0000 ± 0.0005 g), dissolved completely in deionized water, transferred to a 1000 mL volumetric flask, and then diluted to the mark with deionized water, resulting in a 1000 mg/L CIP stock solution.

Preparation and characterization of modified fly ash

The original fly ash was obtained from a thermal power plant in Changchun, China. Initially, it was ground through a 100-mesh sieve, washed with deionized water to neutrality, and then dried for later use. The weight percentages (Wt%) of its components were as follows: C 3.27%, O 42.34%, Na 4.13%, Mg 1.29%, Al 19.33%, and Si 7.23%. Using the original fly ash as the raw material, a Box-Behnken response surface model was employed with the adsorption capacity of CIP (mg/g) as the response value. Microwave power, alkali impregnation concentration, and impregnation time were selected as the three independent factors. Through single-factor experiments, the corresponding gradients were determined as follows: microwave power (320 W, 480 W, 640 W), alkali impregnation concentration (1 mol/L, 1.5 mol/L, 2 mol/L), and impregnation time (2 h, 3 h, 4 h). The fitting results of the model yielded 13 sets of preparation parameters for modified materials, totaling 17 experimental groups with three repetitions each. By comparing the adsorption effects of CIP among the prepared modified materials, the optimal modification conditions were determined. The corresponding modified material (fly ash) was denoted as MFA.

To further elucidate the differences in physico-chemical properties of fly ash before and after modification, the microstructure was evaluated using a scanning electron microscope (SEM, Hitachi SU8010, Japan); the surface functional group distribution was analyzed using a Fourier-transform infrared spectrometer (FT-700, Horiba, Japan); and the crystal structure was analyzed through X-ray diffraction spectroscopy (XRD, Bruker D8 Advance, Germany).

Determination of the pH_{pzc}

To determine the point of zero charge (pH_{pzc}) of FA and MFA, a 0.1 M NaCl solution was prepared and adjusted using 0.1 M NaOH and HCl to set the initial pH (pH_i) from 2 to 12. Subsequently, 0.1 g of FA and MFA were each mixed with 50 mL of the NaCl solution. The mixtures were then agitated at 200 rpm for 48 h, after which the final pH values (pH_f) were measured. A graph was plotted with pH_i on the x-axis and ΔpH ($\Delta pH = pH_f - pH_i$) on the y-axis. The pH_{pzc} for FA and MFA was identified at the point where the curve intersects the x-axis, indicating $\Delta pH = 0$.

Adsorption experiments

A 0.1000 g of FA and MFA were each weighed into 50 mL centrifuge tubes, to which 30 mL of CIP solution (solid-to-liquid ratio of 1:300) was added to conduct adsorption tests. The pH of the CIP solution was adjusted

to 3–11 using 0.1 M NaOH or 0.1 M HCl to find the optimal pH for the experiments. Under the same solid-to-liquid ratio conditions, the solution's pH was adjusted to 6, and samples were taken at intervals ranging from 5 to 1440 min to determine the adsorption kinetics. With the pH set at 6 and a solid-to-liquid ratio of 1:300, the initial concentration of CIP was adjusted between 20 and 140 mg/L, and temperatures were set at 15, 25, and 35 °C to evaluate the effects of fly ash modification on CIP adsorption using isothermal thermodynamics. The concentration of Na^+ ions was varied (0.01, 0.05, 0.1, 0.15, 0.2 M), selecting a concentration of 0.1 M for three types of cations (Na^+, Ca^{2+}, Al^{3+}) to determine the impact of ionic strength and different ions on the adsorption capacity of fly ash. All experiments were performed in triplicate. After adsorption, the solutions were centrifuged using a high-speed centrifuge (10,000 rpm) for 10 min, then filtered through a 0.45 μm filter.

CIP concentration in the solutions was determined using high-performance liquid chromatography (LC-20AT, Shimadzu, Japan). The operating conditions included a column temperature of 40 °C and a mobile phase consisting of 0.1% solution (acetonitrile: water = 20:80). The flow rate was set to 0.2 mL/min with a detection wavelength of 277 nm and a retention time of 4 min.

Data processing

The adsorption amount (Q_a) and removal rate are calculated using the following formulas:

$$Q_a = \frac{(C_0 - C_e)V}{m} \tag{1}$$

$$\text{Remove Rate} = \frac{(C_0 - C_e)}{C_0} \times 100\% \tag{2}$$

where Q_a indicates adsorption capacity (mg/g); V is the volume of the solution (L); m is the mass of the adsorbent (g); C_o and C_e indicates the initial and equilibrium concentrations of the contaminant in the solution (mg/L), respectively.

The data are fitted using the pseudo-first-order Eq. (3) and pseudo-second-order Eq. (4) kinetic models, described by the equations:

$$\lg(Q_e - Q_t) = \lg Q_e - k_1 \cdot t \tag{3}$$

$$\frac{t}{Q_t} = \frac{1}{k_2 \cdot Q_e^2} + \frac{t}{Q_e} \tag{4}$$

where Q_e indicates the equilibrium adsorption capacity (mg/g); Q_t indicates the adsorption capacity at time (t) (mg/g); k_1 and k_2 are rate constants for the pseudo-first-order and pseudo-second-order kinetic models, respectively (min and ((mg/g)/min).

The Langmuir Eq. (5) and Freundlich Eq. (6) isotherm models are used to fit the adsorption data with the following equations:

$$Q_e = \frac{Q_m \cdot K_L \cdot C_e}{1 + K_L \cdot C_e} \tag{5}$$

$$\lg Q_e = \lg K_f + \frac{1}{n} \lg C_e \tag{6}$$

where C_e indicates the concentration of CIP at equilibrium in the solution (mg/L); Q_e indicates the equilibrium adsorption amount (mg/g); Q_m indicates the maximum adsorption capacity (mg/g); K_L is the Langmuir constant, indicative of the affinity of adsorption sites for CIP (L/mg); K_f and n are the Freundlich constants; K_f ((mg/g)/L) relates to adsorption capacity and n indicates the intensity of the adsorption.

The effect of temperature on the equilibrium adsorption coefficient is analyzed using the Gibbs free energy equation:

$$\Delta G^0 = -RTlnK \tag{7}$$

$$\Delta G^0 = \Delta H^0 - T\Delta S^0 \tag{8}$$

where T indicates the absolute temperature (K); R is the universal gas constant (8.314 J/(K/mol)); K is the equilibrium adsorption constant; ΔG^0, ΔH^0 and ΔS^0 indicates the standard Gibbs free energy, enthalpy, and entropy changes (KJ/mol), respectively.

Results and discussion

Preparation and characterization of modified fly ash

Response surface optimization for the preparation of modified fly ash

The preparation of MFA optimized by Box-Behnken response surface model showed significant results in the adsorption of CIP, as indicated in Table 1. The multivariate regression fitting using Design Expert software version 11 revealed a quadratic polynomial regression equation between alkali concentration, microwave power, and soaking time, and the CIP adsorption amount.

Number of tests	Alkali to ash ratio	Calcination temperature/°C	Calcination time/h	Adsorption amount/mg/g
1	1.4	300	4	18.81
2	1.4	400	3	19.29
3	1.3	400	2	17.29
4	1.5	400	2	19.21
5	1.3	400	4	18.27
6	1.5	400	4	18.62
7	1.4	400	3	19.32
8	1.4	500	2	18.67
9	1.5	500	3	18.90
10	1.4	400	3	19.33
11	1.4	500	4	18.74
12	1.4	400	3	19.29
13	1.4	300	2	18.38
14	1.3	300	3	17.63
15	1.3	500	3	17.02
16	1.5	300	3	17.99
17	1.4	400	3	19.32

Table 1. Response surface design and adsorption amount of CIP.

The variance analysis showed that the model's F-value was significantly high at 771.09, suggesting a strong fit to the experimental data with a P-value less than 0.0001. This confirms the significance of the regression model. The lack-of-fit was not significant with a P-value greater than 0.05, validating the model's appropriateness for the experimental data. Moreover, the linear effects of the model's variables A (alkali concentration), B (microwave power), and C (soaking time) were highly significant. The quadratic effects of these variables and their interaction terms (AB, AC, BC) were also significantly impactful on CIP adsorption.

To examine the impact of the three factors and their interactions on CIP adsorption, response surfaces and contour plots (Fig. 1) were analyzed while holding other factors constant. It was observed that alkali concentration and soaking time notably influence the CIP adsorption rate. Increasing both factors enhanced CIP adsorption up to a point after which adsorption decreased. This trend could be due to a full reaction of SiO_3–Al_2O_3 in the fly ash with the alkali, activating more adsorption sites. As alkali concentration increased, the vitreous structure within the fly ash was completely disrupted, which led to the collapse of pore structures and blockage or destruction of adsorption sites, thus decreasing the adsorption capacity[30]. The ideal adsorption conditions for CIP on modified fly ash corresponded to an alkali concentration of 1.40–1.58 mol/L and a soaking time of 2.66–3.34 h, which achieved the optimal adsorption of CIP. Based on the operability, the optimal modification conditions for fly ash were established at an alkali concentration of 1.5 mol/L, soaking time of 3 h, and microwave power of 480 W, achieving an adsorption capacity of 12.49 mg/g.

Characterization of modified fly ash

The SEM images of FA and MFA are shown in Fig. 2. The surface of FA appears relatively smooth with fewer undulations, exhibiting uneven particle sizes and lacking deep pore structures and cavity-like voids, attributed to the presence of abundant amorphous glassy phases on the surface of FA. In contrast, MFA after microwave and NaOH modification displays a rough and uneven surface with abundant pores and distinct layered structures. This is because the glassy phase structure on the surface of FA is gradually melted and contracted into irregular spherical shapes after microwave modification, leading to the fracture of Si–O and Al–O bonds in the internal structure of fly ash, which promotes the layering of the fly ash surface and opens up the internal structure. Meanwhile, the glassy phase structure of aluminum silicate such as Si_2O_3 on the surface of fly ash reacts with NaOH, causing the dissolution of SiO_2 and Al_2O_3 from the glassy phase[31], thus destroying the glassy phase structure, increasing its specific surface area, and releasing the active functional groups inside the fly ash[32]. This process exposes active adsorption sites, enhancing the specific surface area and active sites of MFA, thereby increasing its adsorption capacity for CIP[21].

The X-ray diffraction (XRD) patterns of FA and MFA are depicted in Fig. 3. Both FA and MFA exhibit similar peak patterns, showing prominent diffraction peaks of quartz and mullite near $2\theta = 25.25°$, 35.31°, 37.15°, 43.79°, and 57.66°. This indicates that the crystalline structure on the surface of modified fly ash has not undergone significant changes, and no new crystal structures have been generated[33]. However, specific diffraction peaks show a decrease in intensity, suggesting a decrease in crystallinity. This implies that the crystalline structure on the surface of modified fly ash has been disrupted, leading to an increase in surface porosity and the number of adsorption sites, thereby enhancing the adsorption capacity for CIP.

The FT-IR spectra of FA and MFA are depicted in Fig. 4. The absorption peak at 980.16 cm^{-1} corresponds to the asymmetric stretching vibration peak of SiO_4 in FA, while the peak at 898.08 cm^{-1} corresponds to the deformation vibration peak of tetrahedral hydroxyl groups (Al_2OH) in FA. After NaOH modification, peak shifts occur, indicating the formation of new amorphous Si–O–Si and Si–O–Al network structures, which weaken

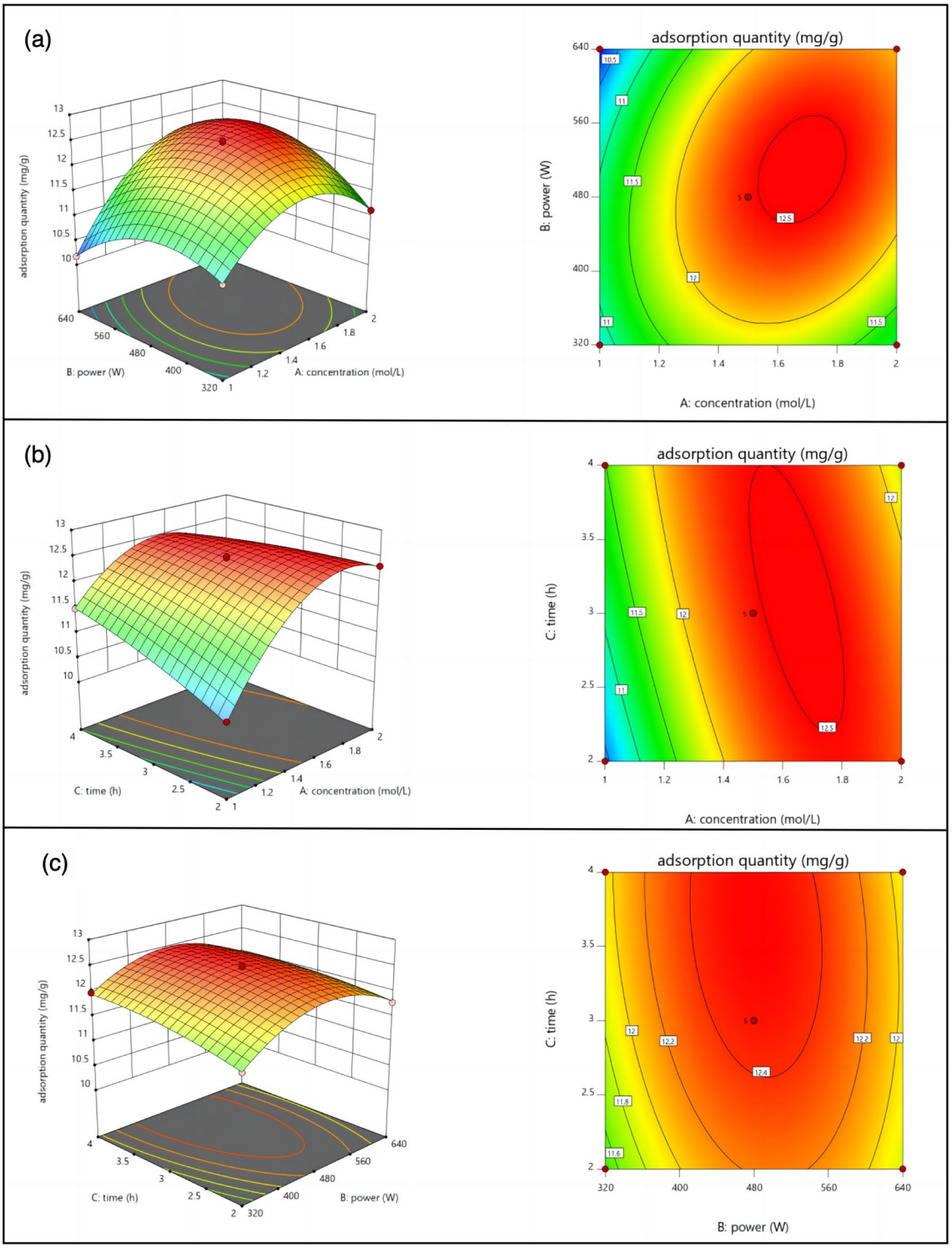

Fig. 1. Effect of base concentration and microwave power (**a**), alkali concentration and soaking time (**b**), microwave power and immersion time (**c**) on the adsorption of CIP in solution.

molecular order and enhance adsorption capacity[34]. Additionally, the characteristic peak near 1651.86 cm^{-1} corresponds to the bending vibration band of H–O–H.

Compared to FA, MFA exhibits a more pronounced hydroxyl O–H absorption peak at 3416.68 cm^{-1} due to the introduction of –OH groups through NaOH modification. The asymmetric stretching vibration peak in MFA becomes sharper and shifts, and the vibration band near 1572.67 cm^{-1} significantly increases, indicating possible destruction of Al–O and Si–O bonds in MFA after NaOH modification[30]. From the comparison in Fig. 4A and B, it can be observed that the peak positions before and after CIP adsorption are generally similar[35]. However,

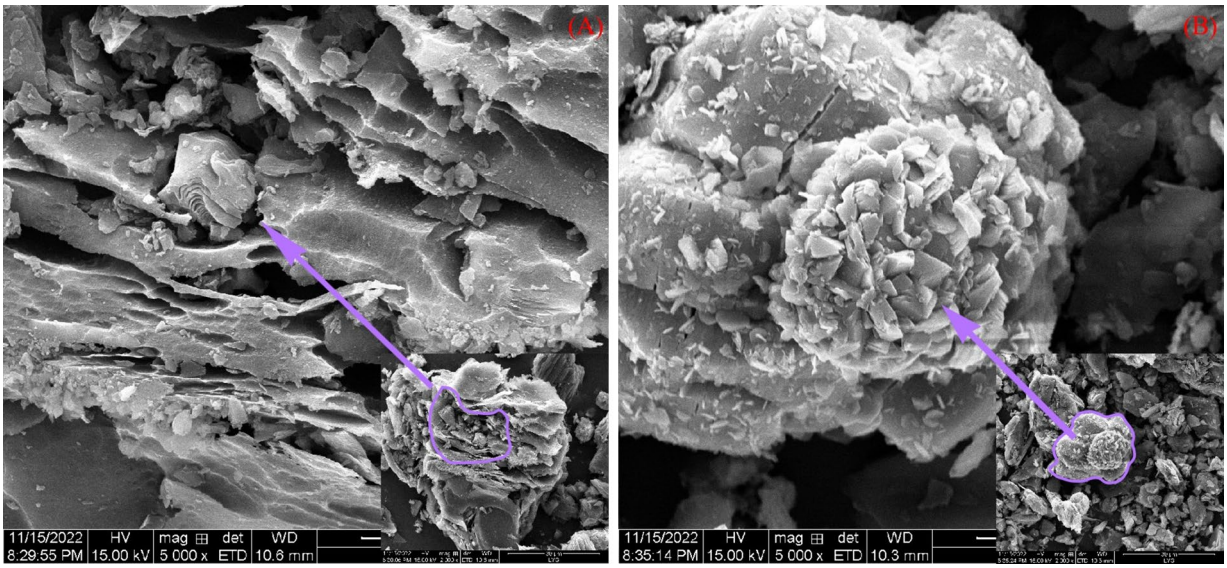

Fig. 2. The scanning electron microscopy image of fly ash (**A**) and modified fly ash (**B**).

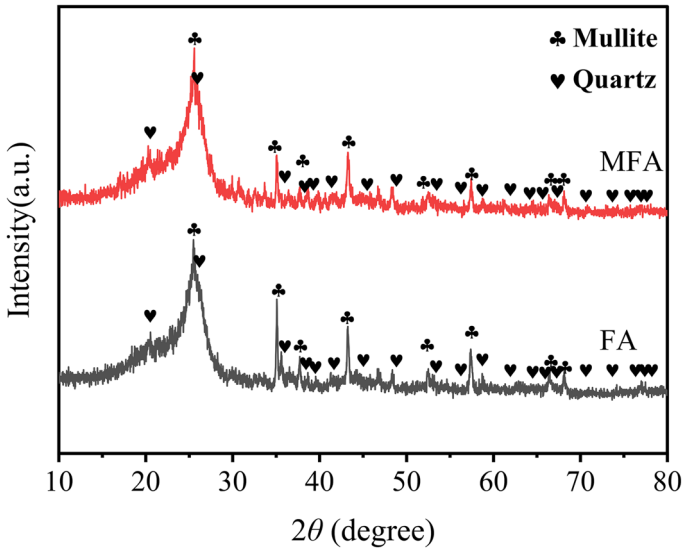

Fig. 3. The X-ray diffraction patterns of fly ash and modified fly ash.

the absorption peaks at 3416.68 cm^{-1}, 2359.70 cm^{-1}, and 1651.86 cm^{-1} show varying degrees of attenuation after CIP adsorption, indicating changes in the corresponding functional group content.

Adsorption characteristics

The influence of initial pH on CIP adsorption

The pH of the solution significantly influences the surface charge of FA and MFA, consequently affecting their adsorption of CIP. As observed in Fig. 5, within the tested pH range of 3–11, the adsorption capacity of both FA and MFA for CIP exhibited an increasing trend followed by a decrease, reaching peak values at pH 6, with maximum adsorption capacities of 9.61 and 12.67 mg/g, respectively. Variations in solution pH result in protonation of functional groups in CIP and alterations in the surface charge of the fly ash. CIP is an ionic organic compound containing both amine and carboxyl functional groups, with dissociation constants of 6.18 and 8.32, respectively[36]. At pH values ≤ 6.18, the amine groups in CIP become protonated, leading to its existence as a cation (CIP^+). Between pH 6.18 and 8.32, CIP exists in a zwitterionic form ($CIP^{\pm}$), while at pH values ≥ 8.32, the carboxyl groups deprotonate, resulting in its existence as an anion (CIP^-)[37]. Metal oxides such as alumina and iron oxide in FA release metal ions (e.g., Al^{3+}, Fe^{3+}, etc.) upon dissolution or decomposition, and these ions can complex with carboxyl and nitrogen heterocyclic groups in CIP molecules, and the porous structure and large specific surface area of FA provide the possibility of CIP adsorption. CIP molecules can be immobilized on the FA surface by physisorption and chemisorption, further promoting the formation of complexes[38].

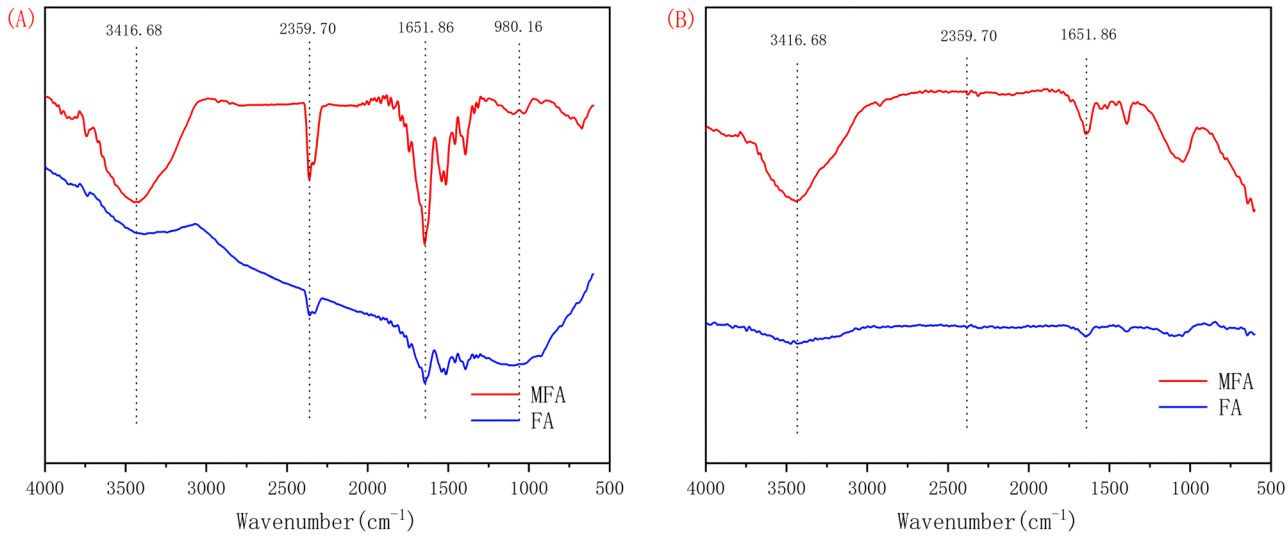

Fig. 4. The FT-IR spectra of fly ash and modified fly ash (**A**), and adsorbed ciprofloxacin (**B**).

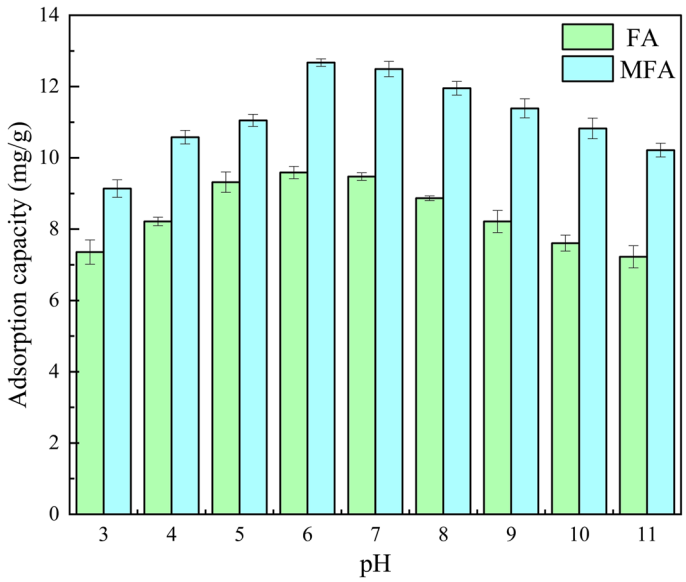

Fig. 5. Effect of pH on adsorption capacity of FA and MFA.

As depicted in Fig. 6, the point of zero charge (pH_{pzc}) for FA and MFA is determined to be 7.18 and 7.53, respectively, indicating positive surface charge at pH values below the respective values and negative surface charge at pH values above them[39]. This indicates that the surface charge of FA becomes positive at pH values below 7.18 and negative at pH values above 7.18, while the surface charge of MFA becomes positive at pH values below 7.53 and negative at pH values above 7.53. At pH values below 6 or above 8, there exists electrostatic repulsion between CIP and FA/MFA. When the background solution pH is between 6 and 7, the material surface carries a positive charge; at pH values between 7 and 8, the material surface carries a negative charge. Therefore, FA and MFA easily adsorb CIP zwitterions at pH values between 6 and 8. Under alkaline conditions, the material surface carries a negative charge, leading to an increase in the concentration of CIP^{-}, thereby enhancing the electrostatic repulsion with FA and MFA. Additionally, competition exists between OH^{-} and CIP^{-} in the solution, weakening the adsorption capacity.

Based on the proportion of zwitterionic CIP, the maximum adsorption capacity of FA and MFA for CIP should occur at pH values of 7.18 and 7.53, respectively. However, the experimental results obtained in this study show that the maximum adsorption occurs at pH 6. This indicates that the adsorption process of CIP by fly ash primarily involves electrostatic interactions, surface adsorption, surface film diffusion, and intra-particle diffusion, as well as other mechanisms such as pore filling and surface complexation[40].

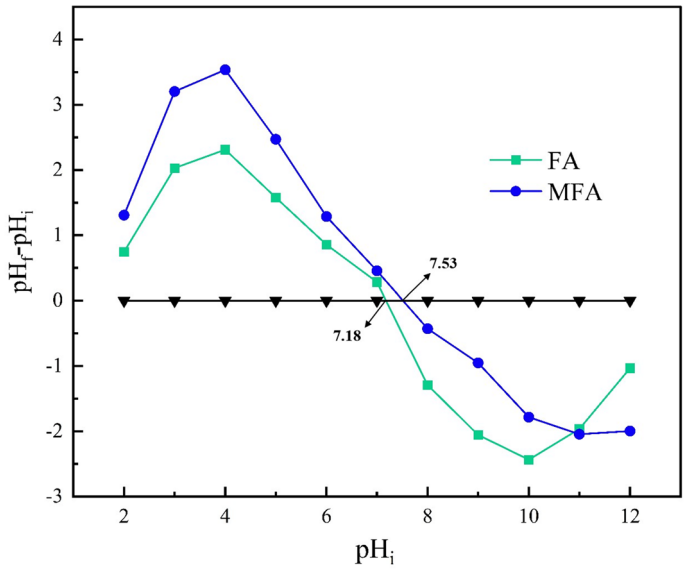

Fig. 6. The pHpzc of fly ash and modified fly ash.

Adsorption kinetics

The adsorption curves and variations of FA and MFA on CIP are shown in Fig. 7 and Table 2. When the adsorbent dosage was 0.1000 g and the initial concentration of CIP was 100 mg/L, the adsorption process of FA and MFA on CIP was divided into rapid adsorption stage, slow adsorption stage, and adsorption equilibrium stage[41,42]. In the initial 0–120 min, it was the rapid adsorption stage, during which the adsorption amounts of CIP by FA and MFA accounted for 89.48% and 96.41% of the total adsorption, respectively. This could be attributed to the abundant porous structure on the surface of FA, providing numerous adsorption sites for CIP at the early stage

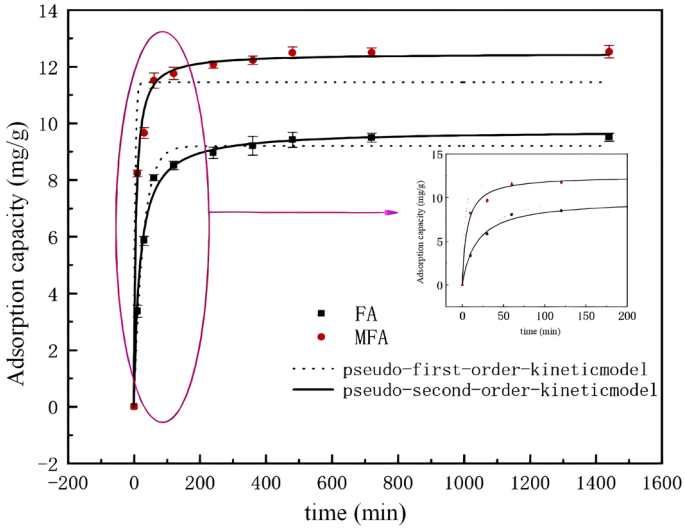

Fig. 7. The adsorption kinetics and fitting curve of CIP.

	10 min	30 min	60 min	120 min	240 min	360 min	480 min	720 min	1440 min
FA	3.37 ± 0.21a	5.86 ± 0.16a	8.08 ± 0.11a	8.51 ± 0.15a	8.96 ± 0.2a	9.21 ± 0.33a	9.42 ± 0.27a	9.5 ± 0.16a	9.51 ± 0.14a
MFA	8.23 ± 0.12a	9.66 ± 0.15ab	11.51 ± 0.27ab	11.76 ± 0.22b	12.08 ± 0.13b	12.23 ± 0.15ab	12.49 ± 0.21ab	12.5 ± 0.17ab	12.53 ± 0.23ab

Table 2. Adsorption of FA and MFA on CIP. The data in the table are mean ± standard deviation, and different letters after the data in the same column indicate significant differences between different treatments ($p < 0.05$).

of adsorption. Compared with FA, MFA exhibited a higher adsorption capacity, indicating that under the action of microwave and NaOH, MFA formed more porous structures on its surface, leading to an increase in surface area. After 480 min of adsorption, the adsorption equilibrium stage was reached, with the equilibrium adsorption amounts of FA and MFA on CIP being 9.51 and 12.53 mg/g, respectively.

To further explore the adsorption kinetics mechanism of FA and MFA, this study employed the pseudo-first-order kinetic equation and pseudo-second-order kinetic equation to fit the data, as shown in Table 3. From the table, it can be observed that both the pseudo-first-order and pseudo-second-order kinetic equations can effectively fit the adsorption kinetics of CIP. However, the pseudo-second-order kinetic equation exhibited better fitting with higher correlation coefficients, with R^2 values of 0.9947 and 0.9930, respectively. The theoretical equilibrium adsorption capacities were also closer to the experimental values. This suggests that the adsorption process of FA and MFA on CIP involves a composite effect of multiple adsorption mechanisms acting simultaneously.

The adsorption isotherm curve

The adsorption isotherm curves depicting the variation of CIP adsorption by FA and MFA are illustrated in Fig. 8. At the experimental temperature, the adsorption trends of CIP by FA and MFA are nearly identical. The adsorption capacity significantly increases with the increasing initial concentration of CIP. At lower concentrations, the active sites on the surface of the fly ash are relatively abundant, resulting in a faster adsorption rate of CIP. As the concentration continues to increase, the adsorption sites on the fly ash surface gradually reach saturation, leading to a plateau in the adsorption capacity curve. Moreover, at the same initial concentration, the adsorption capacity of both FA and MFA decreases with increasing temperature.

To better analyze the adsorption characteristics of fly ash for CIP, Langmuir and Freundlich models were separately employed to fit the isothermal adsorption data. The Langmuir adsorption model assumes that all adsorption sites are identical and operate independently without influencing each other[43], indicating a monolayer adsorption process[44]. On the other hand, the Freundlich adsorption model is an empirical equation that assumes the adsorption process is reversible and continues indefinitely. The calculated correlation coefficients and various reaction constants for each model are presented in Table 4. As observed from the table, the correlation coefficients of the Langmuir model are higher than those of the Freundlich model, indicating that the Langmuir model is more suitable for describing the adsorption process of fly ash for CIP[45]. Therefore, the adsorption of CIP by fly ash is likely to occur on the surface of the fly ash, primarily in the form of monolayer adsorption[46]. Furthermore, based on the thermodynamic parameters, the values of ΔG and ΔH for FA and MFA at different temperatures are negative, suggesting that the adsorption of CIP on fly ash is a spontaneous exothermic reaction. Additionally, the negative ΔH values imply that the adsorption process releases heat, and the spontaneity of the reaction becomes stronger at lower temperatures, indicating an exothermic process overall.

	Pseudo-first-order			Pseudo-second-order		
	$Q_{e,1}$	K_1	R^2	$Q_{e,2}$	K_2	R^2
FA	9.1950	0.0364	0.9878	9.7373	0.0057	0.9947
MFA	11.4433	0.2576	0.8909	12.4600	0.0135	0.9930

Table 3. The kinetic model parameters for the adsorption of CIP by FA and MFA.

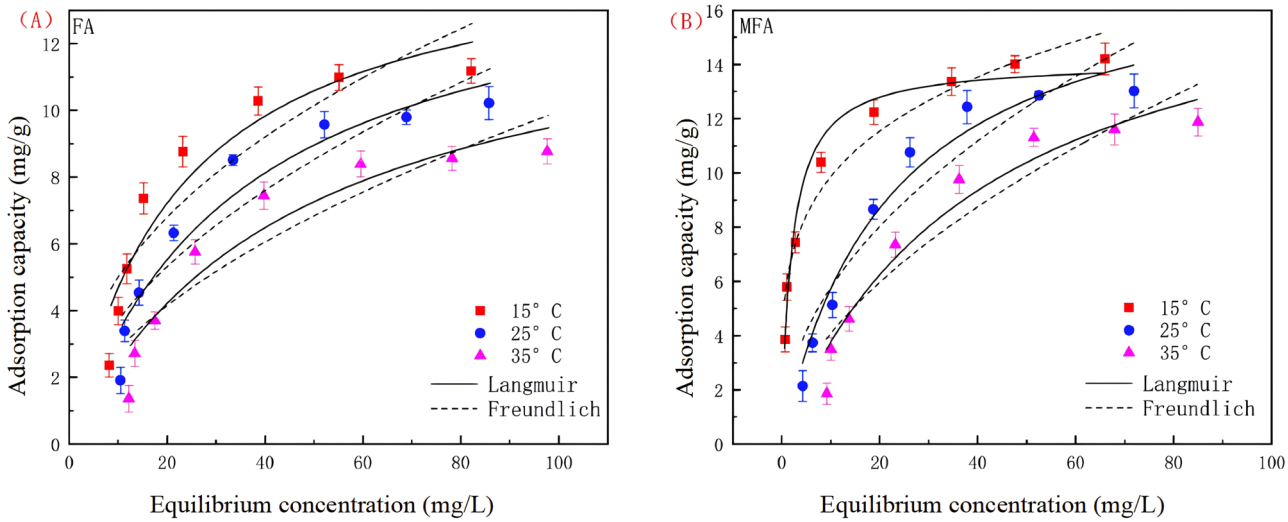

Fig. 8. The adsorption isotherm curve of FA (**A**) and MFA (**B**) to CIP.

	Temperature/K	Freundlich Parameters			Langmuir Parameters			ΔG^0	ΔH^0	ΔS^0
		n	K_f	R^2	Q_m	K_L	R^2			
FA	288	2.3055	1.8573	0.7952	12.7659	0.0453	0.8967	−9.1344	−3.9230	323.84
	298	1.9561	1.1522	0.8543	11.3351	0.0085	0.9226	−5.3120		
	308	1.8404	0.8148	0.8316	9.2649	0.0079	0.9019	−5.3108		
MFA	288	4.3520	5.7949	0.9479	14.9546	0.0747	0.9671	−10.328	−3.0695	319.25
	298	2.0862	1.9047	0.8850	13.6135	0.0092	0.9668	−5.4982		
	308	1.8051	1.1319	0.8852	12.0619	0.0069	0.9463	−4.9460		

Table 4. The adsorption isotherm fitting parameters and thermodynamic parameters for the adsorption of CIP by FA and MFA.

Influence of background solution ionic strength and ion type

The impact of different concentrations of Na^+ addition on the adsorption of CIP by FA and MFA is illustrated in Fig. 9. As observed from the graph, with the increase in ion concentration, the adsorption capacity of CIP by FA and MFA shows a decreasing trend. When the background Na^+ concentration increases to 0.20 M, the adsorption capacity decreases by 33.8% and 24.3% compared to when the Na^+ concentration is 0.01 M. As described in section "3.2.1", the adsorption of CIP by FA and MFA is mainly dominated by cation exchange. When the Na^+ concentration in the solution increases, more Na^+ ions are adsorbed onto the FA and MFA surfaces through electrostatic reactions, occupying the adsorption sites on the material surface, thereby increasing the inhibition of CIP adsorption[47].

In actual wastewater, ions are complex and fluctuating, and the presence of electrolytes affects the interaction between fly ash and the target pollutant CIP. This study investigates the effect of adding 0.1 M Na^+, Ca^{2+}, and Al^{3+} on the adsorption of CIP in FA and MFA, as shown in Fig. 10. It is evident from the graph that the adsorption capacity of CIP by both modified and unmodified fly ash decreases. This can be attributed to the competition between Na^+, Ca^{2+}, and Al^{3+} ions and CIP for the negatively charged adsorption sites on the surfaces of FA and MFA, particularly at pH = 6 where FA and MFA are positively charged, and CIP exists as a zwitterionic species. Additionally, the addition of Na^+, Ca^{2+}, and Al^{3+} ions partially replaces the protons on the surface of FA and MFA, weakening the hydrogen bonds between them and CIP. The relationship between the adsorption capacity and the coexisting ion valence states is as follows: $Na^+ > Ca^{2+} > Al^{3+}$. The smaller the ionic radius, the greater the likelihood of ion exchange occurring, leading to stronger competition.

Adsorption mechanism

Based on the experimental results presented in this study, Fig. 11 illustrates a possible adsorption mechanism. The adsorption process of CIP by fly ash can be explained by pore filling, electrostatic interactions, and chelation. SEM images reveal abundant pore structures on the surface of both FA and MFA. The greater the number of pore structures, the larger the specific surface area, providing more adsorption sites during the adsorption process. According to the adsorption kinetics results, the adsorption of CIP can be explained by a simple filling

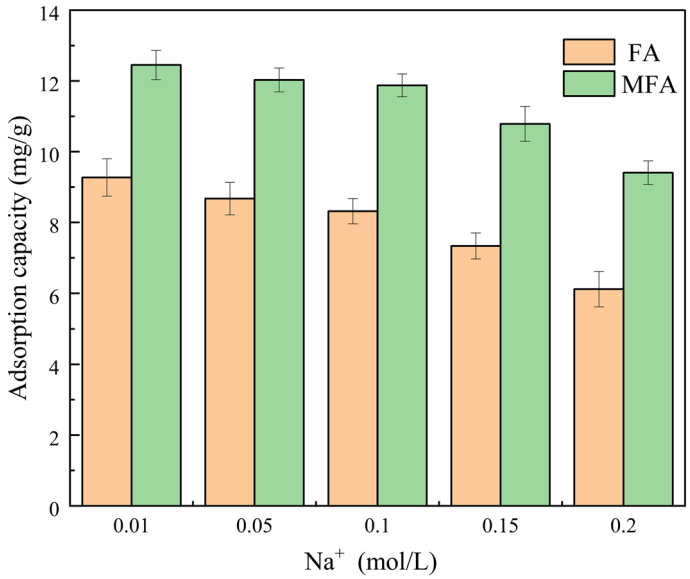

Fig. 9. The influence of background solution ionic strength on adsorption capacity.

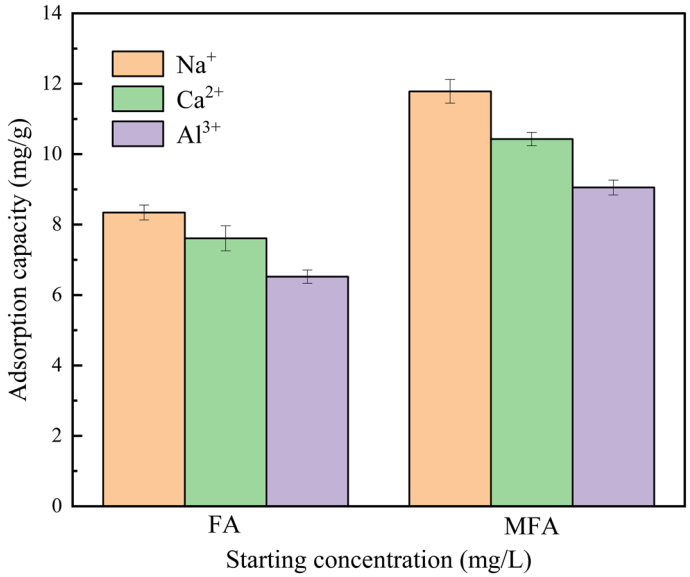

Fig. 10. The impact of background solution ionic type on adsorption capacity.

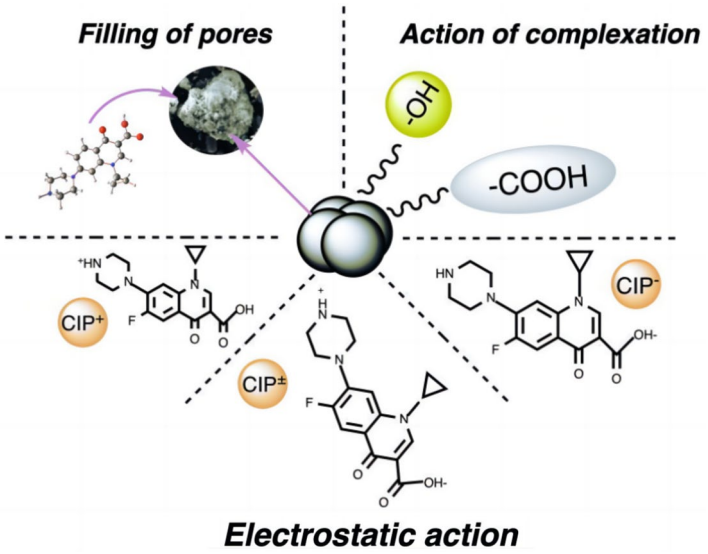

Fig. 11. The mechanism of FA and MFA adsorption of CIP.

mechanism, where adsorption sites are gradually occupied with increasing adsorption time, leading to increased resistance and a decrease in adsorption rate[48]. Moreover, based on the infrared spectra before and after adsorption, the surfaces of the fly ash contain abundant active functional groups (hydroxyl, carbonyl, aldehyde, etc.). FA and MFA have different contents of oxygen-containing functional groups, which undergo a series of chelation reactions with CIP. The pH of the solution directly affects the surface charge properties of both CIP and fly ash. When the pH is lower than the pH_{pzc} (such as pH = 6), the surface of the fly ash carries a positive charge, facilitating electrostatic adsorption with the free CIP in the solution.

Conclusion

This study utilized FA to prepare a novel adsorbent and optimized the preparation conditions of MFA using Box-Behnken response surface design. The optimized conditions were determined as follows: alkali concentration of 1.5 mol/L, immersion time of 3 h, and microwave power of 480 W. Within the pH range of 3–11, the adsorption of CIP exhibited an initial increase followed by a decrease with increasing pH. The maximum adsorption of FA and MFA was observed at pH 6, reaching 9.61 and 12.67 mg/g, respectively. The adsorption kinetics were better described by the pseudo-second-order kinetic equation, with R^2 values of 0.9947 and 0.9930, respectively. The Langmuir model was found to be more suitable for describing the adsorption process. Increasing reaction temperature resulted in decreased CIP adsorption, indicating an exothermic process. The inhibitory effect of ion

types on adsorption followed the order: $Al^{3+} > Ca^{2+} > Na^{+}$. Therefore, in the future treatment of CIP in wastewater, the modified MFA can be added as an ideal adsorbent, MFA has low cost, safe treatment and ideal CIP removal effect, thus achieving the purpose of "treating waste with waste". This study provides a scientific basis for controlling the treatment of CIP in wastewater.

Data availability

The datasets used and/or analysed during the current study available from the corresponding author on reasonable request.

Received: 27 April 2024; Accepted: 22 August 2024
Published online: 27 August 2024

References

1. Girardi, C. *et al.* Biodegradation of ciprofloxacin in water and soil and its effects on the microbial communities. *J. Hazard. Mater.* **198**, 22–30 (2011).
2. Hao, B. *et al.* Tannin foam immobilized with ferric ions for efficient removal of ciprofloxacin at low concentrations. *J. Hazard. Mater.* **414**, 125567 (2021).
3. Tang, J. *et al.* The occurrence and distribution of antibiotics in Lake Chaohu, China: Seasonal variation, potential source and risk assessment. *Chemosphere* **122**, 154–161 (2015).
4. Szekeres, E. *et al.* Investigating antibiotics, antibiotic resistance genes, and microbial contaminants in groundwater in relation to the proximity of urban areas. *Environ. Pollut.* **236**, 734–744 (2018).
5. Pan, M. & Chu, L. Occurrence of antibiotics and antibiotic resistance genes in soils from wastewater irrigation areas in the Pearl River Delta region, southern China. *Sci. Total Environ.* **624**, 145–152 (2018).
6. Tong, L. *et al.* Distribution of antibiotics in alluvial sediment near animal breeding areas at the Jianghan Plain, Central China. *Chemosphere* **186**, 100–107 (2017).
7. Khan, P., Saha, R. & Halder, G. Towards sorptive eradication of pharmaceutical micro-pollutant ciprofloxacin from aquatic environment: A comprehensive review. *Sci. Total Environ.* **919**, 170723 (2024).
8. Sodhi, K. K. & Singh, D. K. Insight into the fluoroquinolone resistance, sources, ecotoxicity, and degradation with special emphasis on ciprofloxacin. *J. Water Process Eng.* **43**, 102218 (2021).
9. Dorival-García, N., Zafra-Gómez, A., Cantarero, S., Navalón, A. & Vílchez, J. L. Simultaneous determination of 13 quinolone antibiotic derivatives in wastewater samples using solid-phase extraction and ultra performance liquid chromatography–tandem mass spectrometry. *Microchem. J.* **106**, 323–333 (2013).
10. Kamal, N., Saha, A. K., Singh, E., Pandey, A. & Bhargava, P. C. Biodegradation of ciprofloxacin using machine learning tools: Kinetics and modelling. *J. Hazard. Mater.* **470**, 134076. https://doi.org/10.1016/j.jhazmat.2024.134076 (2024).
11. Wang, B., Xu, Z. & Dong, B. Occurrence, fate, and ecological risk of antibiotics in wastewater treatment plants in China: A review. *J. Hazard. Mater.* **469**, 133925. https://doi.org/10.1016/j.jhazmat.2024.133925 (2024).
12. Khandaker, S. *et al.* Sustainable approach for wastewater treatment using microbial fuel cells and green energy generation—A comprehensive review. *J. Mol. Liq.* **344**, 117795. https://doi.org/10.1016/j.molliq.2021.117795 (2021).
13. Islam, A. *et al.* Improving valuable metal ions capturing from spent Li-ion batteries with novel materials and approaches. *J. Mol. Liq.* **338**, 116703. https://doi.org/10.1016/j.molliq.2021.116703 (2021).
14. Awual, M. E. *et al.* Ligand imprinted composite adsorbent for effective Ni(II) ion monitoring and removal from contaminated water. *J. Ind. Eng. Chem.* **131**, 585–592. https://doi.org/10.1016/j.jiec.2023.10.062 (2024).
15. Mukherjee, D., Banerjee, S., Ghosh, S. & Majumdar, S. PDMS/ceramic composite membrane synthesis and evaluation of ciprofloxacin removal efficiency. *Korean J. Chem. Eng.* **37**(11), 1985–1998 (2020).
16. Zhao, D., Armutlulu, A., Chen, Q. & Xie, R. Enhanced ciprofloxacin degradation by electrochemical activation of persulfate using iron decorated carbon membrane cathode: Promoting direct single electron transfer to produce 1O2. *Chem. Eng. J.* **437**, 135264 (2022).
17. Rasee, A. I. *et al.* Efficient separation, adsorption, and recovery of samarium(III) ions using novel ligand-based composite adsorbent. *Surf. Interfaces* **41**, 103276. https://doi.org/10.1016/j.surfin.2023.103276 (2023).
18. Berglund, L. A. & Burgert, I. Bioinspired wood nanotechnology for functional materials. *Adv. Mater.* **30**(19), 1704285 (2018).
19. Liu, S. *et al.* Ultra-high adsorption of tetracycline antibiotics on garlic skin-derived porous biomass carbon with high surface area. *New J. Chem.* **44**(3), 1097–1106 (2020).
20. Khandaker, S. *et al.* Functionalized layered double hydroxides composite bio-adsorbent for efficient copper(II) ion encapsulation from wastewater. *J. Environ. Manag.* **300**, 113782. https://doi.org/10.1016/j.jenvman.2021.113782 (2021).
21. Deng, X., Qi, L. & Zhang, Y. Experimental study on adsorption of hexavalent chromium with microwave-assisted alkali modified fly ash. *Water Air Soil Pollut.* **229**(1), 18 (2018).
22. Qi, L. Experimental study on adsorption of Hg(II) with microwave-assisted alkali-modified fly ash. *Powder Technol.* **351**, 153–158 (2019).
23. Jiao, F., Wijaya, N., Zhang, L., Ninomiya, Y. & Hocking, R. Synchrotron-based XANES speciation of chromium in the oxy-fuel fly ash collected from lab-scale drop-tube furnace. *Environ. Technol.* **45**, 6640–6646. https://doi.org/10.1021/es200545e (2011).
24. Hasan, M. M. *et al.* Facial conjugate adsorbent for sustainable Pb(II) ion monitoring and removal from contaminated water. *Colloids Surf. A Physicochem. Eng. Asp.* **673**, 131794. https://doi.org/10.1016/j.colsurfa.2023.131794 (2023).
25. Xu, W., Wang, H. & Zhu, T. Mercury removal from coal combustion flue gas by modified fly ash. *J. Environ. Sci.* **25**, 393–398 (2013).
26. Hossain, M. T. *et al.* Simultaneous toxic Cd(II) and Pb(II) encapsulation from contaminated water using Mg/Al-LDH composite materials. *J. Mol. Liq.* **368**, 120810. https://doi.org/10.1016/j.molliq.2022.120810 (2022).
27. Selvam, M. S. & Balasubramanian, P. Emerging trends and research frontiers of biochar derived through microwave assisted pyrolysis: A scientometric review. *Bioresour. Technol. Rep.* **24**, 101601. https://doi.org/10.1016/j.biteb.2023.101601 (2023).
28. Gupta, V. K., Jain, C. K., Ali, I., Sharma, M. & Saini, V. K. Removal of cadmium and nickel from wastewater using bagasse fly ash-a sugar industry waste. *Water Res.* **37**, 4038–4044 (2003).
29. Chen, J. *et al.* Comparison of adsorption characteristics of acid-base modified fly ash to norfloxacin. *Spectrosc. Lett.* **53**, 416–429 (2020).
30. Huang, X. *et al.* Potential of removing Cd(II) and Pb(II) from contaminated water using a newly modified fly ash. *Chemosphere* **242**, 125148 (2020).
31. Khandaker, S. *et al.* From industrial jute fibre spinning wastes to biofibre-reinforced plastics. *Mater. Chem. Phys.* **313**, 128586. https://doi.org/10.1016/j.matchemphys.2023.128586 (2024).
32. Woolard, C. D., Strong, J. & Erasmus, C. R. Evaluation of the use of modified coal ash as a potential sorbent for organic waste streams. *Appl. Geochem.* **17**(8), 1159–1164 (2002).

33. Li, X. *et al.* Adsorption of norfloxacin from wastewater by biochar with different substrates. *Environ. Geochem. Health* **45**(6), 3331–3344 (2023).
34. Pan, X., Liu, J., Zhang, D. & Yu, H. Formation and transition of calcium aluminate and calcium silicate compounds from pre-synthesized mullite in low-calcium system by solid-state reaction. *Ceram. Int.* **46**(10), 16583–16589 (2020).
35. Li, X., Liu, T., Han, X., Li, Y. & Ma, X. Removal of heavy metals lead and ciprofloxacin from farm wastewater using peanut shell biochar. *Environ. Technol. Innov.* **30**, 103121 (2023).
36. Peng, X. *et al.* Preparation of a graphitic ordered mesoporous carbon and its application in sorption of ciprofloxacin: Kinetics, isotherm, adsorption mechanisms studies. *Microporous Mesoporous Mater.* **228**, 196–206 (2016).
37. Hassan, J. *et al.* Assessment of heavy metals accumulation by vegetables irrigated with different stages of textile wastewater for evaluation of food and health risk. *J. Environ. Manag.* **353**, 120206. https://doi.org/10.1016/j.jenvman.2024.120206 (2024).
38. Tong, F. *et al.* Heavy metal-mediated adsorption of antibiotic tetracycline and ciprofloxacin on two microplastics: Insights into the role of complexation. *Environ. Res.* **216**, 114716. https://doi.org/10.1016/j.envres.2022.114716 (2023).
39. Li, X., Jiang, Y., Liu, T., Yuan, M. & Ma, X. Effects of aging methods on the adsorption of antibiotics in wastewater by soybean straw biochar. *J. Sci. Food Agric.* **104**(1), 468–478 (2024).
40. Nguyen, V.-T. *et al.* Adsorption of norfloxacin from aqueous solution on biochar derived from spent coffee ground: Master variables and response surface method optimized adsorption process. *Chemosphere* **288**, 132577 (2022).
41. Jiang, Y. *et al.* Phosphorus adsorption characteristics and release risk in saline soils: A case study of Songnen Plain, China. *Front. Plant Sci.* **14**, 1302763 (2023).
42. Awual, M. R. *et al.* Ligand based sustainable composite material for sensitive nickel(II) capturing in aqueous media. *J. Environ. Chem. Eng.* **8**(1), 103591. https://doi.org/10.1016/j.jece.2019.103591 (2020).
43. Hossain, M. S. *et al.* Benign separation, adsorption, and recovery of rare-earth Yb(III) ions with specific ligand-based composite adsorbent. *Process Saf. Environ. Prot.* **185**, 367–374. https://doi.org/10.1016/j.psep.2024.03.026 (2024).
44. Waliullah, R. M. *et al.* Optimization of toxic dye removal from contaminated water using chitosan-grafted novel nanocomposite adsorbent. *J. Mol. Liq.* **388**, 122763. https://doi.org/10.1016/j.molliq.2023.122763 (2023).
45. Sheikh, M. C. *et al.* Toxic cadmium(II) monitoring and removal from aqueous solution using ligand-based facial composite adsorbent. *J. Mol. Liq.* **389**, 122854. https://doi.org/10.1016/j.molliq.2023.122854 (2023).
46. Hasan, M. N. *et al.* Assessing sustainable lutetium(III) ions adsorption and recovery using novel composite hybrid nanomaterials. *J. Mol. Struct.* **1276**, 134795. https://doi.org/10.1016/j.molstruc.2022.134795 (2023).
47. Sun, C. *et al.* Low-cost eggshell-fly ash adsorbent for phosphate recovery: A potential slow-release phosphate fertilizer. *Water Res.* **255**, 121483 (2024).
48. Hasan, M. M. *et al.* Sustainable ligand-modified based composite material for the selective and effective cadmium(II) capturing from wastewater. *J. Mol. Liq.* **371**, 121125. https://doi.org/10.1016/j.molliq.2022.121125 (2023).

Acknowledgements

This work was supported by the Jilin Science and Technology Development Program Project (20220203073SF).

Author contributions

Tonglinxi Liu and Wen Liu performed the writing work on the article, Tonglinxi Liu, Hanyu Wang, Yushan Lan and Xinyue Li performed the data processing work on the article. Shengmin Zhang, Yujun Wang and Huiqing Liu checked the structure of the article. Tonglinxi Liu, Wen Liu, Xinyue Li, Hanyu Wang, Yushan Lan, Shengmin Zhang, Yujun Wang and Huiqing Liu are agreed on the publication of the article.

Competing interests

The authors declare no competing interests.

Additional information

Correspondence and requests for materials should be addressed to S.Z. or Y.W.